THE UNIVERSITY of EDINBURGH

Edinburgh Research Explorer

Experimental study of tunnel segmental joints subjected to elevated temperature

Citation for published version:
Yan, Z, Shen, Y, Zhu, H & Lu, Y 2016, 'Experimental study of tunnel segmental joints subjected to elevated temperature', *Tunnelling and Underground Space Technology*, vol. 53, pp. 46-60. https://doi.org/10.1016/j.tust.2016.01.005

Digital Object Identifier (DOI):
10.1016/j.tust.2016.01.005

Link:
Link to publication record in Edinburgh Research Explorer

Document Version:
Early version, also known as pre-print

Published In:
Tunnelling and Underground Space Technology

General rights
Copyright for the publications made accessible via the Edinburgh Research Explorer is retained by the author(s) and / or other copyright owners and it is a condition of accessing these publications that users recognise and abide by the legal requirements associated with these rights.

Take down policy
The University of Edinburgh has made every reasonable effort to ensure that Edinburgh Research Explorer content complies with UK legislation. If you believe that the public display of this file breaches copyright please contact openaccess@ed.ac.uk providing details, and we will remove access to the work immediately and investigate your claim.

OPEN ACCESS

Download date: 12. Oct. 2024

*Manuscript
Click here to view linked References

Experimental Study of Tunnel Segmental joints Subjected to Elevated Temperature

Zhiguo Yan [a,b,c] , Yi Shen [a,b,c], Hehua Zhu [a,b,c], Yong Lu[d]

[a] *State Key Laboratory of Disaster Reduction in Civil Engineering, Tongji University, 1239 Siping Road, Shanghai 200092, China*

[b] *Department of Geotechnical Engineering, Tongji University, 1239 Siping Road, Shanghai 200092, China*

[c] *Key Laboratory of Geotechnical and Underground Engineering of the Ministry of Education, Tongji University, 1239 Siping Road, Shanghai 200092, China*

[d] *Institute for Infrastructure and Environment, School of Engineering, University of Edinburgh, Edinburgh EH9 3JL, UK*

Abstract

Segmental joints present a weak link in the tunnel lining both structurally (due to its low stiffness) and non-structurally (high risk of water leakage); therefore the behaviour of the lining joints has a significant effect on the performance of the shield TBM tunnel lining. Segmental joints are thus a particular concern when the tunnel lining is exposed to high temperature in the case of a tunnel fire. This paper presents an experimental study on the behaviour of TBM tunnel joints in fire under different mechanical loading and boundary conditions, and with both the normal reinforced concrete (RC) segments and hybrid fibre reinforced concrete (HFRC) segments. Totally thirteen jointed specimens were constructed at a scale of 1:3 and tested. Eleven specimens were exposed to a HC (Hydrocarbon) curve and mechanically loaded to failure either under-fire or post-fire, while two specimens were tested in ambient temperature to provide benchmark data. The results demonstrate that the initial loading conditions have a significant effect on the jointed segments during and after fire, and this is closely related to different rate of degradation of concrete in different stress state under high temperature. In general, the resistance capacity of both RC and HFRC joints increased with axial force. The use of HFRC material provided good spalling resistance.

Keywords: Shield TBM tunnel; Lining segmental joints; Fire test; Hybrid fibre reinforced concrete

1. Introduction

In 2005, a small fire broke out in a shield TBM (Tunnel Boring Machine) tunnel construction site of Shanghai Metro Line 8. The upper part of about 430-metre long tunnel lining segments was affected by elevated temperature. More seriously, concrete spalling damage occurred in a region of 16.8 m long, and the maximum damage thickness of the lining concrete was 25 mm (Yan et al., 2012). The incident reminds the engineering community that tunnel fire is a real risk not only to the safety of tunnel users but also to the structural integrity of the tunnel itself. As a matter of fact, several major tunnel fires occurred in the past and they involved severe damage to the tunnel structure in addition to human casualties. **Table 1** gives a list of over a dozen of major tunnel fire accidents throughout the world in the last few decades.

The shield TBM tunnel lining is a special steel–concrete composite structure assembled by individual member segments through lining joints. As a weak link of the tunnel lining due to its low stiffness, and a major source of water leakage, the behaviour of the lining joints significantly affects the performance of the shield TBM tunnel, and it is even more so in the event of high temperature. For instance, in the case of metro shield TBM tunnel linings in soft ground with high water pressure, fire can trigger the failure of the joint seal, causing tunnel lining leakage and even water gushing into the tunnel.

Most previous studies on the TBM tunnel joints have been concerned with the mechanical behaviour of the joints under ambient temperature. Jointed lining has a smaller maximum bending moment capacity than non-jointed lining (Teachavorasinskun and Chub-Uppakarn, 2010). With a certain level of the bending moment a loss of contact can develop on one side of the joint, and this results in nonlinear behaviour which is closely dependent on the axial stress (Arnau and Molins, 2011; Blom, 2002; Molins and Arnau, 2011). The development of the opening angle of the joint affects the rotational stiffness of

the joint (Do et al., 2013). The load eccentricity is also a key parameter affecting the capacity of the joint. In cases where failure is governed by the maximum compressive stress of the concrete in the compressive zone of the joint, ultimate loads decrease as the load eccentricity increases (Zhang and Koizumi, 2007).

For tunnel joints in a fire condition, only limited research work has been reported in the literature. From a full-scale experiment on actual RC metro shield TBM tunnel linings exposed to a standard ISO834 curve (Yan et al., 2012), it was found that the opening angles and gaps of the tunnel lining joints considerably increased while the flexural stiffness of the tunnel lining joints deteriorated under elevated temperatures. In another experimental study (Yan et al., 2013), models of jointed shield TBM tunnel lining rings were tested under a HC (Hydrocarbon) curve. The results indicated that the behaviour and configuration of the lining joints had a significant effect on the mechanical performance, the dynamic internal force redistribution, and the failure pattern of the lining rings when exposed to high temperature. The tests included RC and steel fibre reinforced concrete (SFRC) segments, but only three specimens were tested for each of these two materials.

Many factors contribute to the deterioration of a tunnel lining structure in fire, and concrete spalling and material degradation are two major factors. In recognition of this, attention has been brought to the use of hybrid fibre reinforced concrete (HFRC) with a mixture of steel and polypropylene (PP) fibres. PP fibres melt at approximately 160–170 ˚C; although this would result in a certain reduction in the residual strength of the composite material, the melting of the PP fibres within the heated concrete is believed to mitigate the buildup of pore pressure and thus improve the spalling resistance of the concrete material (Chen and Liu, 2004; Kalifa et al., 2001; Pliya et al., 2011; Suhaendi and Horiguchi, 2006). The complementary functions of polypropylene fibres (improving spalling resistance) and steel fibres (ensuring ductility and crack resistance) make HFRC a promising composite

material for a desirable fire performance (Yan et al., 2013; Rodrigues et al., 2010).

The work presented in this paper is focused on the experimental behaviour of TBM tunnel joints in fire under different mechanical loading and boundary conditions, and with both RC and HFRC materials. Totally thirteen tunnel joint specimens at a scale of 1:3 were constructed and tested, including six RC specimens and seven HFRC specimens. Eleven of the specimens were exposed to a HC (Hydrocarbon) curve, while two were tested in ambient temperature to provide benchmark data. Among the eleven specimens exposed to fire, six were loaded to failure under fire, and five were loaded post fire. Other parameters investigated include the initial loading condition and the level of the axial force.

2. Experimental program

2.1 Materials and specimens

The standard configuration of the test specimens was an assembly of two lining segments connected to each other by bolts as in a real tunnel lining ring. Reduced scale (1:3) specimens were employed in the experiments. This scale level allows the use of normal RC and HFRC materials with realistic segment details, and at the same time reduces the demands on the test facilities considerably.

The test lining segments were 300 mm in width and 120 mm in thickness. The arc length of each segment was 1.53 m, and the average radius was 990 mm, cf. **Fig.1**. To match an actual metro shield TBM tunnel lining segment, details of the hand hole, the longitudinal tongue and groove of the lining segment were retained in the test specimens. The connection between the two segments was made by two curved M-10 Grade-5.8 bolts. Some non-structural details in the real tunnel lining, such as the rubber waterstop and flexible gasket of the lining joints, were omitted.

The mix design of the plain concrete is shown in **Table 2**. The properties of the

polypropylene (PP) and steel fibres as provided by the manufacturer are presented in **Table 3** and **Table 4**, respectively. In the HFRC specimens, the volume fraction of steel fibre and PP fibre was 78 kg/m^3 and 2 kg/m^3, respectively. The choice of a relatively high steel fibre volume was made in order to ensure an appropriate level of the flexural strength in the absence of main steel reinforcement. According to some previous research on HFRC (Libre et al., 2011), the volumetric ratio of the steel fibres in the present study is still within a practical limit. The measured standard cube strengths of the plain concrete and the hybrid fibre reinforced concrete, tested at the age of 28 days under ambient temperature, were 69.8 MPa and 61.1 MPa, respectively. Furthermore, for the RC lining segments, the main reinforcing bars (hot-rolled rebar) were 10 mm in diameter and the concrete cover was 15 mm thick (cf. **Fig.1**).

To ensure consistent production quality, all test segments were fabricated by a professional concrete plant. The age of the concrete at the time of testing the specimens is listed in **Table 5**.

2.2 Test procedure

A newly-developed thermo-mechanical test system for tunnel lining segments under elevated temperatures, as shown in **Fig.2**, was used for the experiment. This system contains two combustors of industrial grade, and the heating-up procedure can be controlled automatically by a programmable controller. The peak temperature in the furnace can reach 1200 ˚C and the maximum heating rate is about 250 ˚C/min. The whole system is capable of simulating different fire scenarios, including high rate heating and high peak temperature, while the test specimens can be subjected to different mechanical loading and boundary conditions.

An international standard HC curve was employed in the experiment to simulate the heating phase of a fire (CEN, 2002), which may be expressed as:

$$T(t) = 20 + 1080\,(1 - 0.325e^{-0.167t} - 0.675e^{-2.5t}) \quad (1)$$

where t is time (in minutes) and $T(t)$ is the gas temperature inside the furnace (in ˚C).

The peak temperature inside the furnace was set at 1100 ˚C, and the heating duration was 60 minutes. The furnace was then turned off, and the specimens were gradually cooled to the ambient temperature. A comparison between the measured temperature curve and the standard HC curve is shown in **Fig. 3**.

As illustrated in **Fig. 2**, the two-segment assembly was supported at both ends by rollers allowing free rotation. Each roller is then attached to a horizontal actuator, such that different levels of the horizontal force, which is equal to the axial force at the joint, were maintained during different tests.

Based on the load equivalent principle and the mechanical characteristics of actual tunnel lining, the mechanical loads were applied in the vertical direction at two distribution points by a single hydraulic actuator, and in the horizontal direction at each support separately by a hydraulic actuator (cf. **Fig. 1**). A load cell was attached to each hydraulic actuator to monitor the load levels. This loading system enables any desired combinations of bending moment and axial force at the segment joint to be achieved. It is noted that because of the curved shape of the specimens, the horizontal force applied at the end supports also produces a bending moment at the middle joint, and this has been taken into account in the design and calculation of the bending moment at the joint.

For the present investigation, the main aim of the loading scheme was to subject the joint to fire and/or mechanical loads until failure under a given level of axial compression. For this purpose, the general mechanical loading schemes include an initial loading phase in which the desired axial force was installed via the horizontal actuators attached at the end supports. In this process, the vertical load was also applied proportionately so that a desired bending moment level at the joint (denoted by M_c) was achieved as part of the initial

condition. Further mechanical loading in the test-to-failure phase was applied by increasing the vertical load only, and this effectively resulted in increasing the sagging (positive) bending moment at the joint under a constant axial force. Here we define sagging (positive) bending moment as the moment that produces concave bending at the middle joint of a specimen, and hogging (negative) bending moment produces raised bending at the middle joint.

Most of the specimens were tested with an axial force level of 40 kN, except two pairs of RC and HFRC specimens which were tested under 20 kN and 60 kN axial force, respectively. An axial force of 40 kN is equivalent to a nominal level of axial compression of the top segmental joint of a tunnel with a buried depth of 10 m in the Yangtze River Delta Region (where the stratum is constituted mainly by the saturated mucky soft clay).

Table 5 summarises the test conditions for all the specimens. In all, three different fire and mechanical loading conditions (LC) were considered, namely:

(i) Loading Case 0 (LC0): ambient temperature test. Two specimens, one for RC (designated as RC1) and one for HFRC (HFRC1), were tested under a constant axial force of 40 kN to provide benchmark responses for comparison. The loading was implemented in two phases. In the first phase a 40 kN axial force with a zero bending moment at the joint was established in an initial loading process as described earlier. The second phase was to load the specimens by increasing the vertical load (or effectively the bending moment) until failure.

(ii) Loading Case 1 (LC1): ultimate bending strength under fire. The test segments were heated following the standard HC curve, without any initial loading. After approximately 40 minutes of heating, the specimens were mechanically loaded to failure to investigate the ultimate strength under high temperature. Three pairs of specimens were subjected to LC1 tests, including RC2/HFRC2 (under a constant horizontal force of 20kN),

RC3/HFRC3 (under a constant horizontal force of 40kN) and RC4/HFRC4 (under a constant horizontal force of 60kN).

(iii) Loading Case 2 (LC2): residual bending strength after exposure to fire. In the first step, the test segments were mechanically loaded to a prescribed initial (service) load level with an axial force of 40 kN and bending moment M_c ranging from -4 to 2 kN.m, and then subjected to a complete heating (following HC curve) and cooling process. In the second step, the specimens were loaded to failure by increasing the vertical load while maintaining the horizontal force, to investigate the ultimate strength and bending stiffness after exposure to high temperature. Five specimens were tested with LC2, including RC5/HFRC5 (initially loaded by a sagging moment of 2 kN.m in the first step); RC6/HFRC6 (initially loaded by a hogging moment of 2 kN.m in the first step); and HFRC7 (initially loaded by a sagging moment of 4 kN.m in the first step).

The temperature distribution, mid-span deflection, vertical load and horizontal reaction forces at the supports were measured in the tests (cf. **Fig.1**). Two measuring sections were arranged to measure the temperature within each of the two adjoining segments in a specimen. For each of the temperature measuring sections, five K type thermocouples were installed at 10 mm, 30 mm, 60 mm, 90 mm and 120 mm from the heating surface across the thickness of the linings, respectively (cf. **Fig.1**). To avoid disturbance from heat radiation and concrete spalling or cracking, the first thermocouple (closest to the heating surface) was installed at 10 mm into the thickness. The thermocouples were arranged with at least 20 mm spacing along the width of the linings so as to avoid interference between them. To install the thermocouples, small holes (5 mm in diameter) were drilled first from the top surfaces. After cleaning these holes, a small amount of fine aluminum powder was injected into the bottom of the holes to ensure good heat conduction between the concrete and the thermocouples. After installation of the thermocouples, the holes were filled with cement

paste.

LVDTs were employed to measure the vertical deflections at the mid-span and some selected locations, and the horizontal displacements at the supports. In addition, an ultrasonic pulse velocity (UPV) test instrument (called Pundit Lab) was used to examine the quality of concrete. A non-destructive concrete moisture meter was used for measuring the concrete moisture of the segments. A non-contact, high sensitivity infrared radiometer (MikroScan 7600PRO) was used to check up the accuracy of temperature measurement. This device measures the infrared radiation emitted by the target surface and converts this radiation into a two-dimensional image of the temperature distribution on the target surface.

The nominal opening gap and opening angle of the lining joints in the tests can be inferred from a set-up as illustrated in **Fig. 4**. In this set-up a pair of measuring arms was fixed onto the outer surface of segments on the two sides of the joint, and a pair of LVDTs was mounted to the measuring arms at two different distances from the segment surface to measure the relative displacements ΔL_1 and ΔL_2. The opening angle and the opening gap may be determined from the relative displacements by the following equations (Yan et al., 2012):

$$\begin{cases} \theta = 2\arctan\dfrac{\Delta L_1 - \Delta L_2}{2d_1} \\ \Delta_{inside} = (d_2 + H)\dfrac{\Delta L_1 - \Delta L_2}{d_1} - \Delta L_2 \\ \Delta_{outside} = d_2\dfrac{\Delta L_1 - \Delta L_2}{d_1} - \Delta L_2 \end{cases} \tag{2}$$

where θ is the opening angle of the lining joints; Δ_{inside} is the opening gap of the lining joints at the heating surface (in mm); $\Delta_{outside}$ is the opening gap (when the value becomes positive) of the lining joints at the unexposed surface (in mm); d_1 is the distance between two LVDTs (in mm); d_2 is the distance between the second (lower) LVDT and the

unexposed surface (in mm); ΔL_1 and ΔL_2 are the displacement increments of the first and the second LVDT, respectively (in mm); H is the thickness of the tunnel linings (in mm). It should be noted that the joint rotation and gap openings inferred from Eq. 2 included also the differential strain deformation between the inner and outer sides of the specimens over the measuring length. But relatively speaking these strain deformations were generally small as compared to the deformations at the joint gap and therefore they are neglected.

3. General test results and discussion

3.1 Temperature fields

Fig.3 depicts the standard HC curve and the measured curve from the fire tests. The temperature inside the furnace matched the target HC curve satisfactorily. The temperature histories at different depths from the heating surface across the thickness of the lining specimens are presented in **Fig.5**. As can be seen, at different depths concrete reached the highest temperature not at the furnace shut-off time but with a time delay. This was due to the fact that heat continued to conduct from the heated side of the segment to the unheated side after the furnace shut-off. Across the depth the temperature was highest at the nearest inner side (10mm), as can be expected, and it reduced rapidly as the distance to the heated side increased. Taking the temperature at the end of heating (60 min) for example, the temperature at 10mm from the heated side was very close to furnace temperature of 1100 ^{o}C, and reduced to 600 ^{o}C at 30mm and about 300 ^{o}C at 60mm. The temperature profiles between RC and HFRC specimens showed no marked difference.

At the joint the heat flux flowed through the gap and propagated outward, and the flow intensified as the inner side of the joint stretched and the gap opened more widely. As a result, the temperature of the concrete in the vicinity of the joint section was higher than adjacent areas for similar depth. Since a direct observation of the joints during heating was

blocked by the insulation board, we used a thermal infrared imager to capture the heat profile of the specimen right after the shut-off of the combustor. **Fig.6** shows a typical thermal image of the specimens. As can be seen, the joint section area clearly experienced higher temperature and the distribution across the depth was more uniform than a typical segment section away from the joint. Based on thermal data, the average temperature of the joint section was found to be approximately 20% higher than that at a typical lining section.

3.2 Spalling and failure mode of specimens

Pervious fire incidents and laboratory experiments indicate that elevated temperature can cause explosive spalling of concrete (Beard and Carvel, 2005; Both et al., 2003; Zeiml, et al., 2006; Zeiml, et al., 2009). The consequences of spalling on the general performance of the tunnel can vary depending upon the functions concrete lining is designed or expected to fulfil in the tunnel structure. As far as a segment joint is concerned, however, spalling can have a serious effect on the fire resistance of the joint because extensive removal of concrete will undermine the integrity of the joint, and this in turn affects the structural behaviour of the tunnel.

The severity of spalling was inspected after the test. **Fig.7** shows two typical cases of spalling around the handhole of the specimens, one for a RC specimen (RC2) and another for an HFRC specimen (HFRC2). For the RC specimen, the spalling zone expanded to the anchoring end of the bolt with a large piece of concrete removed, and it effectively exposed a part of the steel reinforcement around the handhole. This was a clear evidence of the detrimental effect that spalling can cause on the integrity of the RC joint. In contrast, for HFRC specimens, no visible spalling was found at the joint; and in fact the handhole even maintained intact after the bolt yielded due to mechanical loading. Such a superior spalling resistance in the HFRC specimens is deemed to be attributable to the presence of the polypropylene fibres in the mix of fibres used in the HFRC specimens. Polypropylene

fibres melt at approximately 160–170 ^{o}C within the heated concrete, and this would produce new expansion channels and connect existing internal channels within concrete material (Pliya et al., 2011). As a result, the accumulated water vapour escapes and the build-up of pore pressure inside concrete are alleviated (see e.g. Colombo and Felicetti, 2007).

Three basic modes govern the failure of specimens, namely a) yielding of the joint bolts, b) failure of concrete at the joint, and c) failure of the segment. A summary of the individual failure modes of all test specimens is given in **Table 5**. As far as failure due to yielding of joint bolts is concerned, the failure of the bolts in the ambient cases and that in the under-fire cases exhibited rather different final patterns. The comparisons between the deformed bolts and un-deformed bolts in ambient and under-fire cases are illustrated in **Fig.8**. The bolts of HFRC specimens were highly oxidized and reacted chemically with the concrete contacting with it during fire. This resulted in the bolt showing light grey colour after the test. For cases with concrete failure occurred at the joint, the final distortions of the bolts were severe, as shown in **Fig.8**.

The different failure modes will be discussed further in association with the detailed results concerning the structural behaviour in the next section.

4. Structural behaviour of specimens and effects of fire

4.1 Structural behaviour of joints under ambient temperature (LC0)

As reference cases, the two specimens RCJ1 (reinforced concrete) and HFRCJ1 (hybrid fibre reinforced concrete) tested under ambient temperature were loaded vertically until failure while being subjected to a constant axial force of 40 kN.

Fig.9 (a) and **(b)** show the failure modes of the two specimens. The relationships of vertical load vs. vertical displacement at the joint, and bending moment vs. gap opening are

illustrated in **Fig.10 (a)** and **(b)**. Specimens RCJ1 exhibited a behaviour which was clearly dominated by the bending-rotation at the segment joint, and failed at the joint due to yielding of the curved bolts. As stretching and yielding of the bolts continued, the compression zone reduced, leading to crushing of the top edge concrete at the final stage (**Fig. 9 (a)**).

Specimen HFRCJ1 also exhibited a response pattern similar to RCJ1 for much of the loading range, with visible gap opening at the joint (**Fig.9 (b)**). However, while the bending strength at the joint continuously developed as in RCJ1, the bending moment capacity of the plain HFRC section (without main steel bars) was effectively exhausted, leading to a sudden collapse of the specimen when the vertical load reached about 85 kN. The bending moment at the joint was equal to about 8.68 kN.m, and the maximum bending moment over the segment, which occurred at the vertical loading point, was about 9.8 kN.m.

Standard hand calculations were carried out for the bending moment capacities of the segmental joint, the RC section and the HFRC section at ambient temperature for the three axial force levels. The results are listed in **Table 6**, including the anticipated failure mode for each case. In the calculations the yield strength for the two bolts is assumed to be 640 MPa, the yield strength for the main steel bars for RC is 300 MPa, the compressive strength for the normal concrete is 60 MPa and for HFRC is 65 MPa, and tensile strength for HFRC is 10 MPa.

For an axial force of 40 kN, the bending moment strength is calculated to be 10.4 kN.m for the joints (yielding of the bolts), 18.2 kNm for the RC section (yielding of tension bars), and 8.4 kN.m for the HFRC section (tension failure of HFRC material). These results are very consistent with the test results, and confirm that the failure of RCJ1 was indeed governed by bending of the joint, whereas failure of HFRCJ1 was due to rupture of the HFRC material even though significant joint opening was involved due to stretching of the

curved bolts. The joint did not reach the ultimate strength in HFRCJ1 when the specimen failed.

4.2 Structural behaviour of joints under elevated temperature (LC1)

4.2.1 Deflections and joint deformations under fire

The variation of the vertical deflections measured at the joint location for the RC specimens (RCJ2, RCJ3, RCJ4) and HFRC specimens (HFRCJ2, HFRCJ3, HFRCJ4) with the free heating time are depicted in **Fig.11**. For a comparison, the vertical deflections measured from single segment specimens (i.e., without the joint; details of those tests are omitted here) under a similar fire condition are also included.

As can be observed, for the segments without involving a joint, the mid-span deflection kept increasing downwards (i.e. towards the heating side). This is expected from the differential thermal elongation of specimen intrados and extrados induced by the temperature distribution. For the jointed segments, the vertical deflection at the mid-span (joint location) also increased gradually downwards with increase in temperature for about 13 minutes after ignition; however, this trend was reversed afterwards; the incremental vertical deflections moved upward, resulting in a decrease of the total deflection. The total deflection was almost recovered after about 30 minutes of heating. After that time, the vertical deflections continued to move upward slightly.

The above observed reversal of deflection trend during heating was attributable to the local deformation and gap development at the joint. **Fig.12** shows the rotation and opening gap histories for these specimens tested under elevated temperature. As shown in **Fig.12 (a)**, in the beginning the opening gap increased faster on the inner side than on the outer side. After a period of about 12-13 minutes, the opening gap on the inner side almost maintained at a constant value while the opening gap on the outer side continued increasing. From the

rotation plot shown in **Fig.12 (b)**, the joint appeared to rotate inward slightly and then outward at a faster rate. **Fig.13** illustrates the deflection mechanisms within a single segment and with the bolted joint. During the first period of heating (about 12 min) some uneven thermal elongation of the segmental concrete occurred causing the inner side of the joint to open (the first stage in **Fig.13**). When the difference in the deformation between the bolts and the concrete reached a certain level, the opening gap of the inner side became restricted. Meanwhile, the outer-side concrete continued to expand under intense heating through the gap of the joint, resulting in the rotation of joint turning to a negative value (the second stage in **Fig.13**). Consequently, the increment of the mid-span deflection developed in the opposite (upward) direction and thus the total deflection exhibited a recovery trend.

4.2.2 Resistance, bending moment capacities

Specimen RCJ3 is directly comparable to the reference specimen RCJ1 as the mechanical loading conditions were the same except the fire effect. Similarly HFRCJ3 can be compared with HFRCJ1 directly. **Fig.14** shows the relationships of vertical load vs. vertical displacement and joint bending moment vs. joint opening gap for the two specimens. The final failure patterns are shown in **Fig.9 (a), (b), (e)** and **(f)**.

Under the elevated temperature, specimen RCJ3 exhibited generally similar load-deformation behaviour as RCJ1 and the failure mode was also dominated by yielding of the bolts at the joint until the concrete on the compression edge at the joint region crushed. The loading capacity was governed by the maximum bending moment at the joint, which was 9.04 kN.m as compared to 11.38 kN.m in RCJ1, showing a decrease of about 20%. This decrease of the bending moment capacity may be explained by the reduction of the yield strength of the bolts under the fire effect. According to the temperature measurements discussed in Section 3, the temperature at the location of the bolts during the

load testing phase reached about 400 ^{0}C, and for the bolts made of structural steel the yield strength would generally reduce by 58% under such temperature (CEN, 2005).

Specimen HFRCJ3 performed poorly under fire, and the maximum load capacity in terms of the bending moment developed at the joint location was only 3.45 kN.m as compared to 8.68 kN.m in specimen HFRCJ1 under ambient temperature. The failure mode was controlled by the rupture failure of the HFRC section, which was similar to the failure mode of HFRCJ1. However, the HFRC section had no main steel rebar, so when the section cracked and the thin steel fibres were exposed to high temperature, the bending capacity quickly diminished resulting in an accelerated failure of the specimen.

For another two pairs of specimens which were also tested under elevated temperature but with different levels of axial forces, namely RCJ2 & HFRCJ2 and RCJ4 & HFRCJ4, **Fig.15** shows the vertical load vs. vertical displacement and joint bending moment vs. joint rotation relations. The corresponding final failure patterns are shown in **Fig.9 (c), (d), (g)** and **(h)**. The results are summarized and discussed in what follows.

For specimen RCJ2 which was under a reduced axial force of 20 kN, the response was dominated by the bending rotation at the joint, and consequently the failure was due to yielding of the bolts. The achieved load capacity in terms of the bending moment at the joint was 6.14 kN.m, which was markedly lower than that of RCJ3 due apparently to the lower axial force while in the tensile flexural failure mode. Comparing to the predicted bending strength of the joint section under ambient temperature, i.e. 8.2 kN.m, there was a decrease of about 25%, and this is consistent with the observation from the comparison between RCJ3 and RCJ1 such that the reduction of the strength of the bolts under the elevated temperature was directly responsible for the reduction in the flexural strength under fire. The response in specimen HFRCJ2 with axial force of 20 kN also appeared to have been governed by the bending-rotation of the joint and no fracture occurred in the

HFRC sections. As such, the response in HFRCJ2 was very similar to RCJ2.

Specimen RCJ4 under an increased axial force of 60 kN exhibited a markedly increased resistance capacity as compared to RCJ2 of 40 kN under the same fire condition, with a maximum vertical load of 140 kN comparing to 90 kN, or maximum joint bending moment of 15.26 kN.m comparing to 9.04 kN.m. Whereas this was clearly attributable to the general effect of increased axial force resulting in a reduced tension demand on the bolts, it is interesting to note that the bending capacity exceeded even the predicted joint bending strength under ambient temperature by a significant margin, and the final failure mode shifted to a compression failure at the joint. One possible explanation is thought to be related to the load induced thermal strain (LITS) effect, such that the higher level of compressive stress caused an extra compressive strain due to LITS. The increased compressive strain would have delayed the development of tensile stress in the bolts during the mechanical load phase under fire, while the compressive stress on the compression zone intensified. This resulted in an overall increase of the bending capacity, but at the same time led to accumulation of higher compressive strain on the top side of the joint section, leading eventually to a compressive bending failure of the joint. This phenomenon is worth further investigation in subsequent studies.

Similar situation is believed to have occurred at the joint region of HFRCJ4. The increase of the axial force also enhanced the bending capacity of the HFRC sections. However, the increased bending moment capacity at the HFRC sections tended to be less than the increased bending capacity at the joint; as a result rupture of the HFRC section at the vertical loading point (where maximum bending moment took place) occurred prior to a joint compressive bending failure as in RCJ4.

4.3 Structural behaviour of joints after exposure to fire (LC2)

4.3.1 Deflections and joint deformations under fire

For the specimens tested mechanically to failure after exposure to fire, **Fig.16** shows the vertical deflection and rotation histories during the heating and cooling cycle. The deformations induced by the initial loading, including vertical displacements, rotations and opening gaps, are ignored because they were relatively small. HFRCJ6 is not shown in this figure because some part of the data was lost due to a sudden power failure during the heating-cooling process.

For specimens which were exposed to heating under a sagging moment, namely RCJ5 and HFRCJ5, the vertical displacements appeared to reduce during both heating and cooling phases. On the contrary, for specimens which were subjected to a hogging moment during heating, namely RCJ6 (HFRCJ6 data was missing), the vertical displacement exhibited an increase during the cooling phase. These patterns of deformation illustrated a complex effect of joint opening and the thermal expansion under the two different service load conditions when exposed to fire.

For specimen HFRCJ7 which was subjected to a larger initial sagging moment of 4 kN.m, the deflection increased during the heating phase and then tended to stabilise at around 10 mm. However, the continued penetration of heat into the deeper layer of concrete after the termination of heating resulted in continued weakening of the steel fibres, leading to the eventual failure of this specimen during the cooling phase, before further mechanical loading.

4.3.2 Resistance, bending moment capacities

Fig.17 shows the vertical load vs. vertical displacement and joint bending moment vs. joint rotation relations for RCJ5 & HFRCJ5 and RCJ6 & HFRCJ6**.** The initial load

condition during the heating phases had significant effects on the moment-curvature curves in the post-fire loading tests. For specimens RCJ5 & HFRCJ5 which were subjected to sagging initial moment, the moment-curvature curves in the post-fire loading phase were almost linear until the specimens failed abruptly. On the other hand, for specimens RCJ6 and HFRCJ6 which were initially subjected to a hogging moment during heating, the moment-curvature curves exhibited a bi-linear character, and the stiffness in the first stage appears to be smaller than that in the second stage.

The final failure patterns from post-fire loading tests are shown in **Fig.18**. The severer degradation in specimen RCJ5 at the joint region is clearly noticeable. Although specimen RCJ6 also failed eventually in compression at the joint region, the much less degradation in the compressive concrete from the heating, as also visible from the photo (**Fig. 18(c)**), helped the specimen to show a much higher resistance capacity. The failure patterns in the HFRC specimens tend to show some combined effects and this may be attributed to the characteristics of the HFRC sections in association to the higher uncertainties involved in the ultimate strength as discussed earlier in Section 4.2.

The above effects may be explained as follows. In the cases with an initial sagging moment, the joint opened wider on the heating side and this resulted in quicker heat transfer through the joint to the upper compressive concrete. The compressive concrete degraded under high temperature but consolidation took place at the same time; as a result, when the specimens were loaded in the post-fire testing, the specimens exhibited a stiffened behaviour, but failed in an abrupt manner and at a lower loading capacity due to the degradation of the compressive concrete during heating. On the contrary, in the cases with an initial hogging moment, the heated side was under compression, thus the joint opening on the heating side was reduced which effectively protected the upper layer of concrete in the joint region. When these specimens were subsequently tested under increased vertical

loading, the critical joint region was subjected to reversed sagging moment. The degradation of the concrete at the bottom side resulted in a "softer" behaviour in terms of the bending deformation under the reversed sagging moment, but as the top side concrete was generally intact during the heating phase, the specimens were able to retain their load resistance capacities, as clearly shown in the comparative curves in **Fig. 17**.

5. Conclusions

In this paper, the fire effects on the behaviour of shield TBM tunnel lining segmental joints were investigated experimentally. Two different types of the lining segments were considered, namely normal reinforced concrete (RC) segments and hybrid fibre reinforced concrete (HFRC) segments. The fire effects are examined comprehensively in terms of the temperature distribution, concrete spallation, and the mechanical load-deformation relationships and the final failure modes. The mechanical failure loading tests were conducted for both under-fire and post-fire conditions. Furthermore, different combinations of the axial force and bending moment at the joints were considered. Based on the experimental results, the following conclusions may be drawn:

(1) The presence of the joint allowed the heat flux to flow through the gap and propagate outward. This resulted in a higher temperature region in the concrete in the vicinity of the joint than in adjacent areas at similar depth. Consequently, the deterioration of concrete in the joint region was generally severer, and this in turn affected the strength of the joint as well as the entire unit under mechanical loading, particularly in cases where the final failure was due to concrete compressive failure at the joint.

(2) Whereas in RC specimens typical patterns of spalling were observed under high temperature, in HFRC specimens spalling was almost completely avoided even in the higher temperature joint region. This further confirmed the effect of use of polypropylene

fibres in spalling control under high temperature.

(3) All RC specimens were observed to fail at the joints. For RC specimens tested to failure under high temperature, failure mostly occurred in a tensile bending mode with extensive yielding and joint gap openings before final crushing of concrete at the top side. For specimens tested to failure after the exposure to fire, failure occurred in compressive bending mode at the joints. The initial bending condition during heating had an apparent effect on the post-fire strength. With initial sagging bending moment, the upper layer of concrete at the joint was subjected to high compression, leading to accelerated degradation under high temperature and eventually a much reduced compressive capacity With initial hogging bending moment, the upper layer of concrete at the joint was almost stress free due to combined hogging moment and axial load, thus was less degraded during heating.

(4) While HFRC material exhibited good performance against spalling under high temperature, the HFRC sections appeared to be less resistant to bending, especially under high temperature. This can be attributed to the lack of main steel rebar and the weakness of think steel fibres (and their bond with concrete) when exposed to heating. The results suggest that a minimum amount of main steel rebar should be considered in HFRC lining segments where significant bending could occur.

Further work is required to develop a quantitative method to evaluate the structural strength of jointed segments during and after fire under various representative mechanical loading conditions. The experimental data presented in this paper provides a necessary basis to advance in that direction. Effective ways of protecting and enhancing the joint region against fire is also a topic worthy dedicated investigation.

Acknowledgements

The authors acknowledge the financial supports from the National Natural Science

Foundation of China (51478345, 51578410), the National Basic Research Program of China (973 Program) (2011CB013800), the Shanghai Natural Science Foundation (15ZR1443600), the Shanghai Pujiang Program (14PJD034), and Research Program of State Key Laboratory for Disaster Reduction in Civil Engineering.

References

Arnau O., Molins C. Experimental and analytical study of the structural response of segmental tunnel linings based on an in situ loading test. Part 2: Numerical simulation. Tunnelling and Underground Space Technology 2011; 26: 778-788.

Beard A., Carvel R. The Handbook of Tunnel Fire Safety, London, Thomas Telford Publishing, 2005.

Blom C.B.M. Design philosophy of concrete linings for tunnels in soft soils. Ph.D Thesis. Technische Universiteit Delft, 2002.

Both C., Wolsink G.M., Breunese A.J. Spalling of concrete tunnel linings in fire. In: Proceedings of ITA-AITES 2003 World Tunnel Congress. Netherland: Amsterdam; 2003. 227-31.

Cafaro E, Bertola V. Fires in tunnels: experiments and modelling. Open Thermodynamics Journal, 2010, 4(4): 156-166.

CEN (European Committee for Standardization). Eurocode 1: Actions on structures, EN 1991-1-2(2002).

CEN (European Committee for Standardization). Eurocode 4 – Design of composite steel and concrete structures. EN1994-1-2: 2005 (E)

Chen B., Liu J. Residual strength of hybrid-fibre reinforced high strength concrete after exposure to high temperature. Cement and Concrete Research 2004; 34:1065–9.

Colombo M., Felicetti R. New NDT techniques for the assessment of fire-damaged concrete structures. Fire Safety Journal 2007; 42: 461-72.

Do N., Dias D., Oreste P., et al. 2D numerical investigation of segmental tunnel lining behaviour. Tunnelling and Underground Space Technology 2013; 37: 115-127.

Haack A. Current Safety Issues in Traffic Tunnels. Tunnelling and Underground Space Technology, 2002, 17: 117－127.

Haack A. Latest achievement and perspectives in tunnel safety. Tunnelling and

Underground Space Technology, 2004, 19:305.

ITA (International Tunnelling and Underground Space Association). Guidelines for structural fire resistance for road tunnels, 2005.

Kalifa P., Chéné G., Gallé C. High-temperature behaviour of HPC with polypropylene fibres: From spalling to microstructure. Cement and Concrete Research 2001; 31: 1487-1499.

Khoury G A. Effect of Fire on Concrete and Concrete Structures. Progress of Structure Engineering Material，2000, 2：429-447.

Kim J.H., Lim Y.M., Won J.P., Park H.G. Fire resistant behaviour of newly developed bottom-ash-based cementitious coating applied concrete tunnel lining under RABT fire loading. Construction and Building Materials 2010; 24: 1984-94.

Leitner A. The fire catastrophe in the Tauern Tunnel： experience and conclusions for the Austrian guidelines. Tunnelling and Underground Space Technology，2001，16（1）：217－223.

Libre N.A., Shekarchi M., Mahoutian M. Mechanical properties of hybrid fibre reinforced lightweight aggregate concrete made with natural pumice. Construction and Building Materials 2011; 25: 2458-2464.

Molins C., Arnau O. Experimental and analytical study of the structural response of segmental tunnel linings based on an in situ loading test.: Part 1: Test configuration and execution. Tunnelling and Underground Space Technology 2011; 26: 764-777.

Park S.Y., Oh H.K., Shin Y.S., Oh S.J. A case study on the fire damage of the underground box structures and its repair works. Tunnelling and Underground Space Technology 2006; 21: 328.

Pliya P., Beaucour A.L., Noumowé A. Contribution of cocktail of polypropylene and steel fibres in improving the behaviour of high strength concrete subjected to high temperature. Construction and Building Materials 2011; 25: 1926-1934.

Rodrigues J.P.C, Laím L., Correia A.M. Behaviour of fibre reinforced concrete columns in fire. Composite Structures 2010; 92: 1263-1268.

Schrefler B.A., Brunello P., Gawin D. et al. Concrete at high temperature with application to tunnel fire. Computational Mechanics 2002; 29: 43-51.

Suhaendi L.S., Horiguchi T. Effect of short fibres on residual permeability and mechanical properties of hybrid fibre reinforced high strength concrete after heat exposition. Cement and Concrete Research 2006; 36: 1672-1678.

Teachavorasinskun S., Chub-Uppakarn T. Influence of segmental joints on tunnel lining. Tunnelling and Underground Space Technology 2010; 25: 490-494.

Vianello C, Fabiano B, Palazzi E, et al. Experimental study on thermal and toxic hazards connected to fire scenarios in road tunnels. Journal of Loss Prevention in the Process Industries, 2012, 25(4): 718-729.

Yan Z.G., Zhu H.H., Ju J.W., Ding W.Q. Full-scale fire tests of RC metro shield TBM tunnel linings. Construction and Building Materials, 2012; 36: 484-94.

Yan Z.G., Zhu H.H., Ju J.W. Behaviour of reinforced concrete and steel fibre reinforced concrete shield TBM tunnel linings exposed to high temperatures. Construction and Building Materials 2013; 38: 610-618.

Zeiml M., Leithner D., Lackner R., et al. How do polypropylene fibres improve the spalling behaviour of in-situ concrete? Cement and Concrete Research 2006; 36: 929-942.

Zeiml M., Lackner R., Mang H.A. Experimental insight into spalling behaviour of concrete tunnel linings under fire loading. ACTA Geotechnica 2009; 3:295-308.

Zhang W., Koizumi A. A study of the localized bearing capacity of reinforced concrete K-segment. Tunnelling and underground space technology 2007; 22: 467-473.

Figure

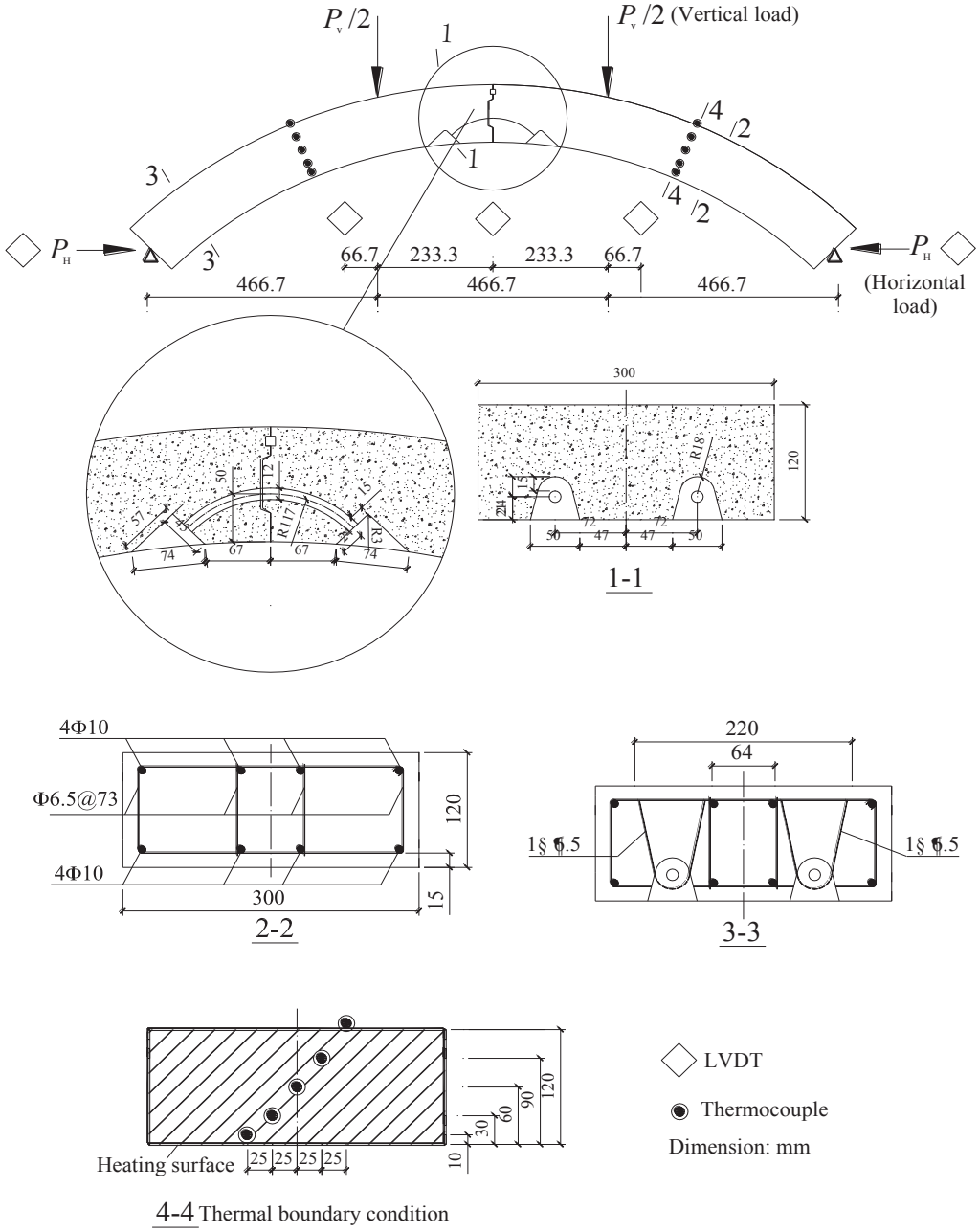

Fig.1. Configuration of joint assembly, reinforcement arrangement for the RC lining segments, and instrumentation

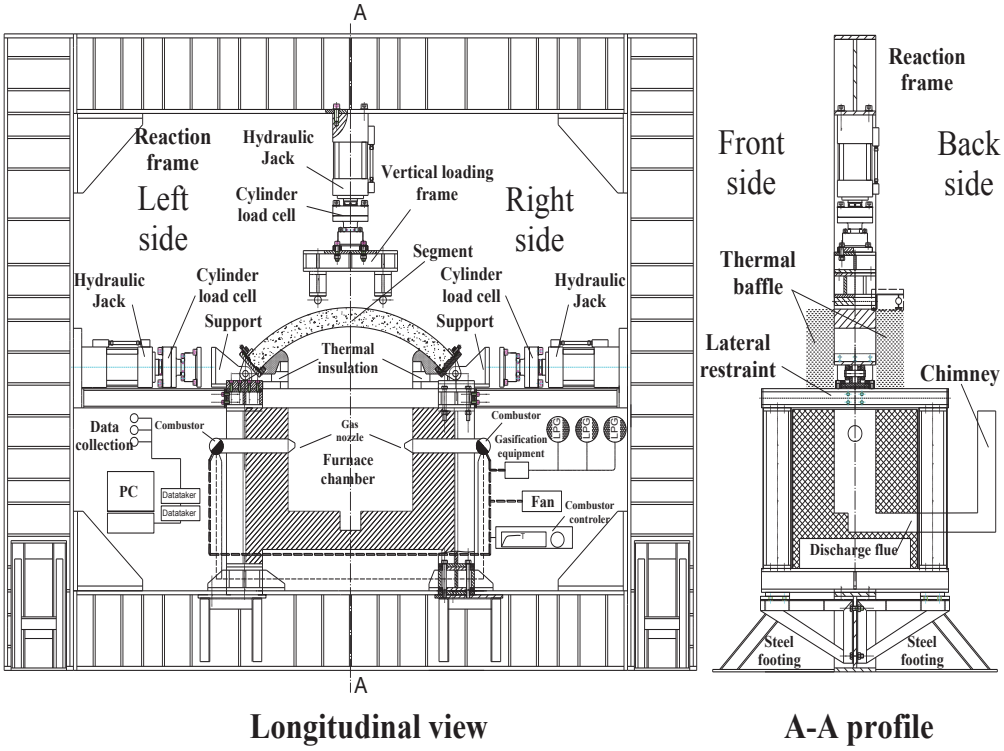

Fig.2. Test setup for combined mechanical and thermal loadings of shield TBM tunnel segments and joints

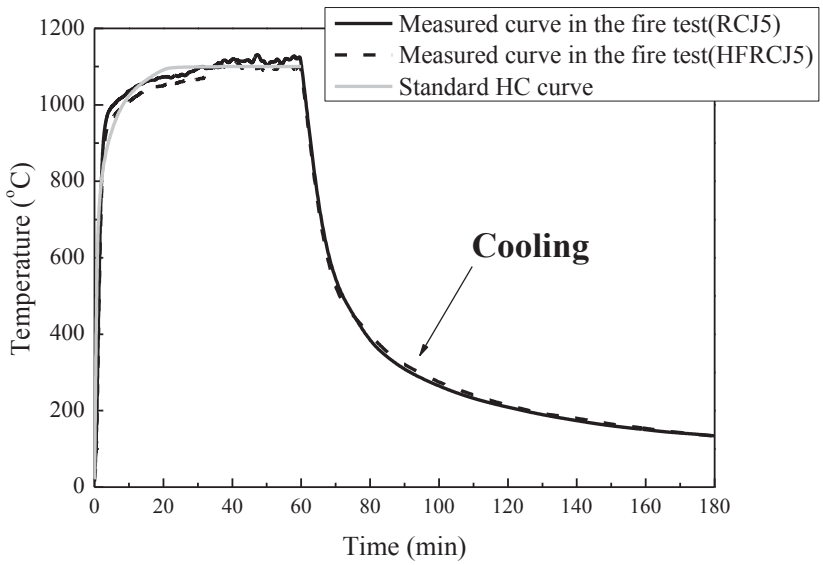

Fig.3. Standard HC curve and the measured curves from the fire tests

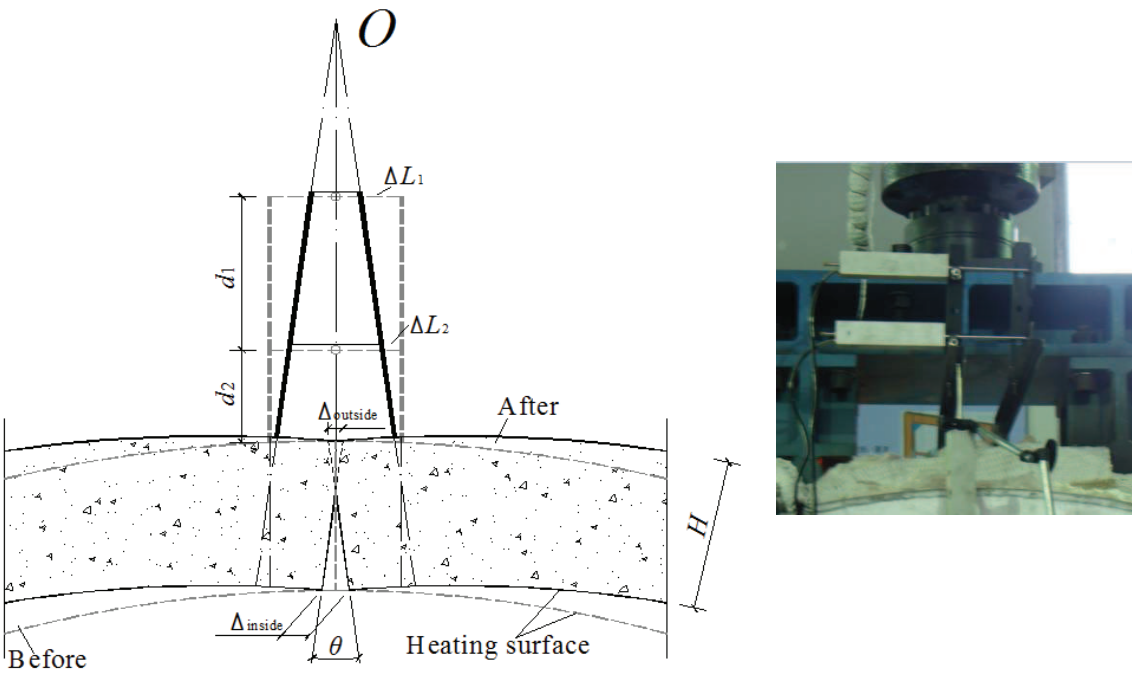

Principle Test set-up

Fig.4. Measurement of opening angle of the lining joints

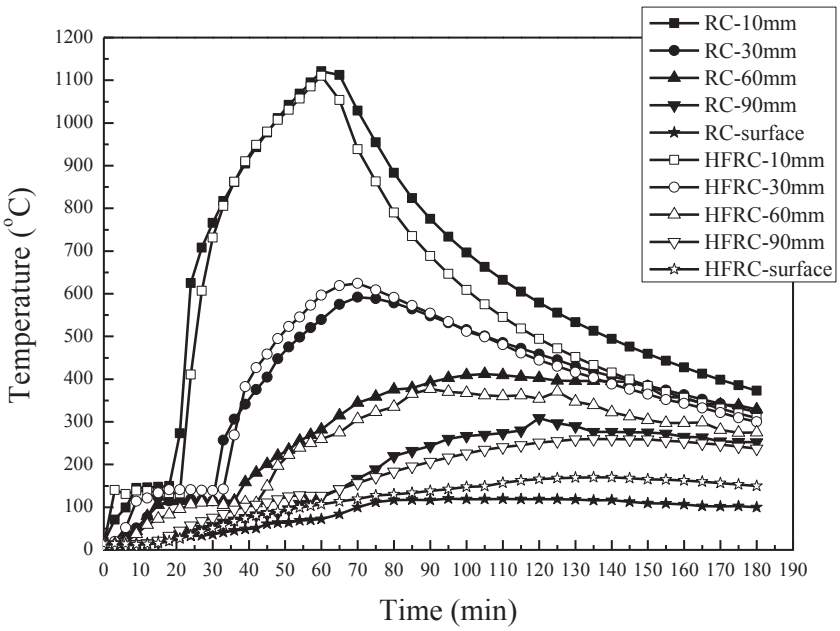

Fig.5. Temperature histories at different depths from the heating surface of the specimens

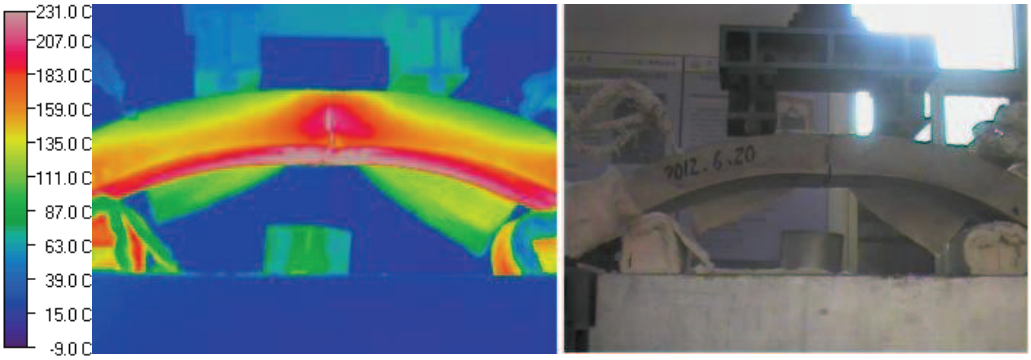

Fig.6. Thermal infrared images of heated specimens

RC2 HFRC2

Fig.7. Spalling conditions around the handhole of RC and HFRC specimens

HFRCJ1

HFRCJ2

RCJ4

RCJ6

Fig.8. Comparison between deformed and original bolts from the specimens involving joint concrete failure

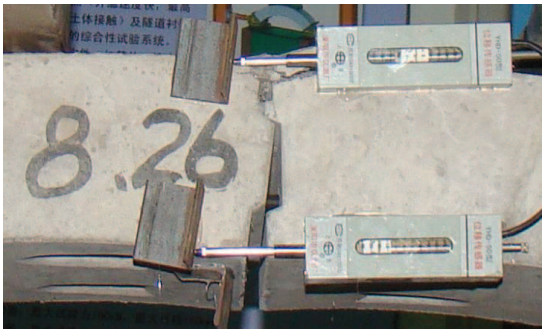

(a) Joint bolts yielding (RCJ1)

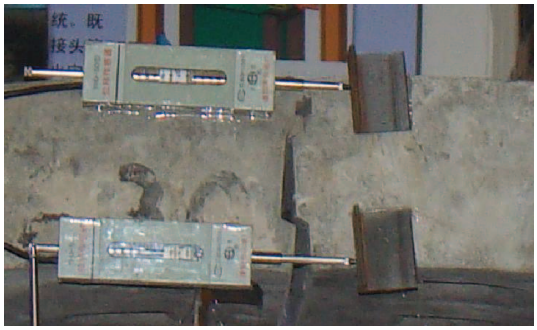

(b) Joint bolts yielding (HFRCJ1)

(c) Joint bolts yielding (RCJ2)

(d) Joint bolts yielding (HFRCJ2)

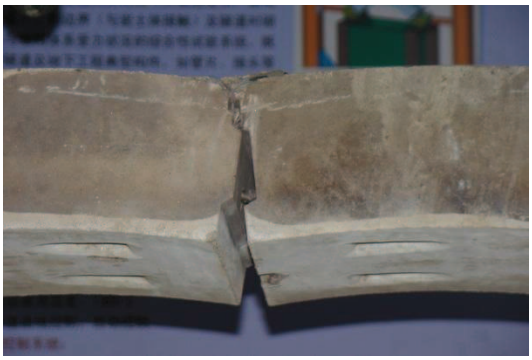

(e) Joint bolts yielding (RCJ3)

(f) Concrete fracture (HFRCJ3)

(g) Joint concrete failure (RCJ4)

(h) Concrete fracture (HFRCJ4)

Fig.9. Failure modes of specimens tested at ambient temperature and under fire

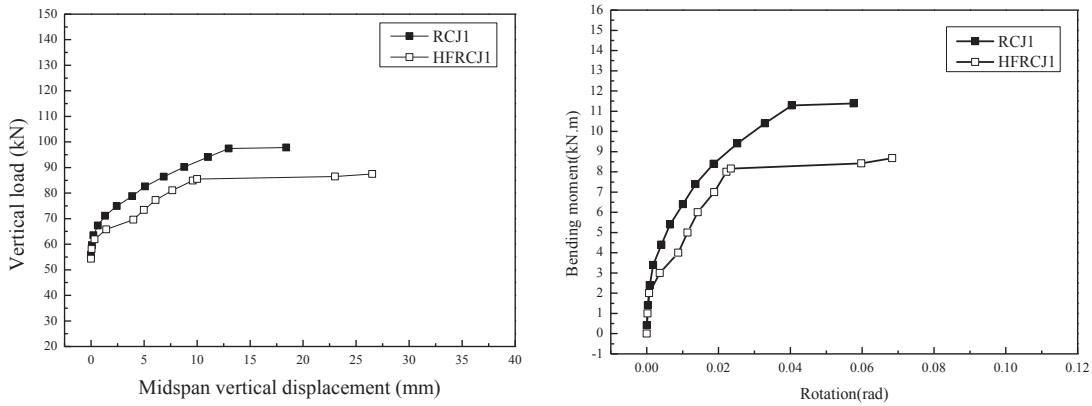

(a) Vertical load vs. vertical displacement (b) Joint bending moment vs. rotation

Fig.10. Load vs. deformation curves for RCJ1 and HFRCJ1 (ambient temperature and P_H=40 kN)

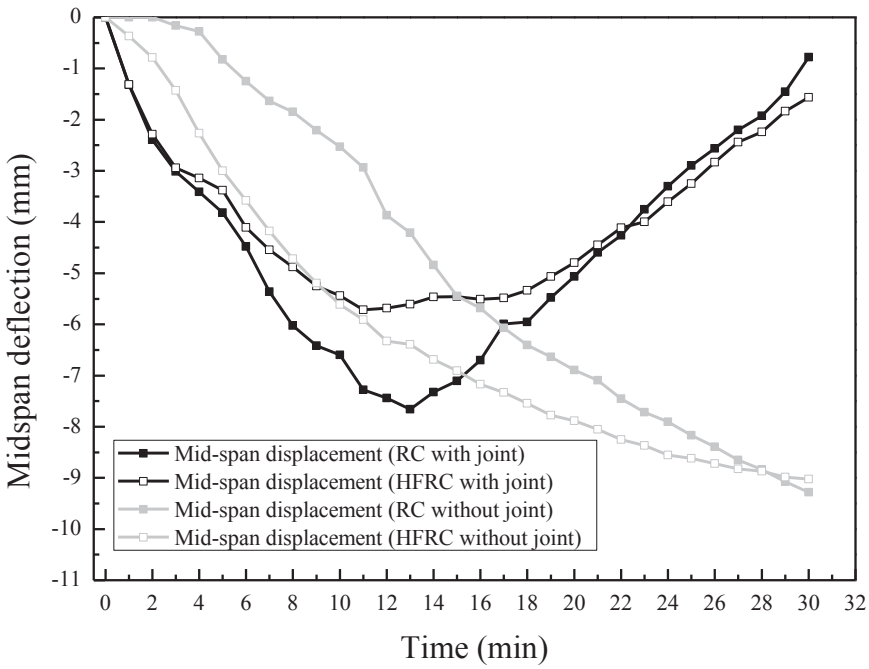

Fig.11. Mid-span deflection histories during heating: comparison between jointed segments and stand-alone segments

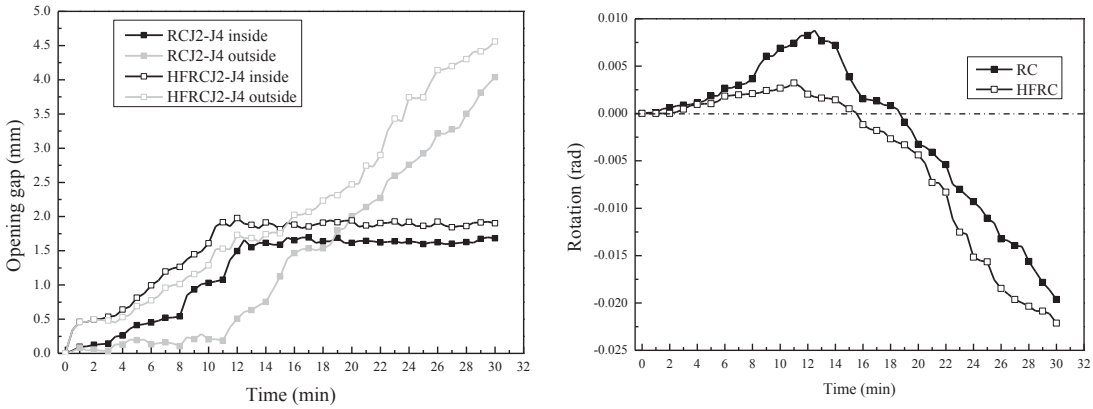

(a) Opening gap (b) Rotation

Fig.12. Rotation and gap opening histories of the under-fire cases

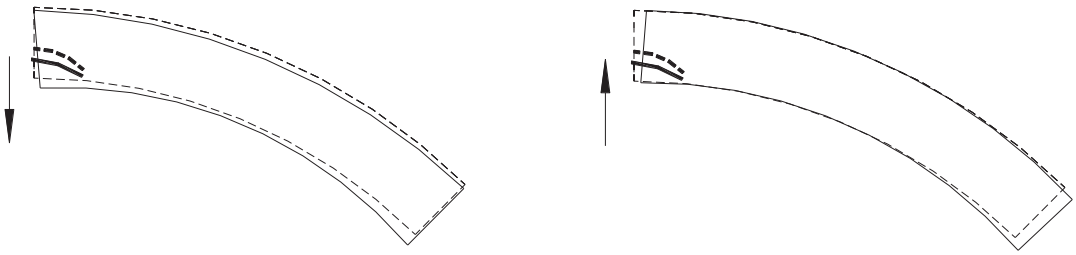

First stage Second stage

Fig.13. Deflection mechanism of single segment and bolted joints (dashed part shows the initial state)

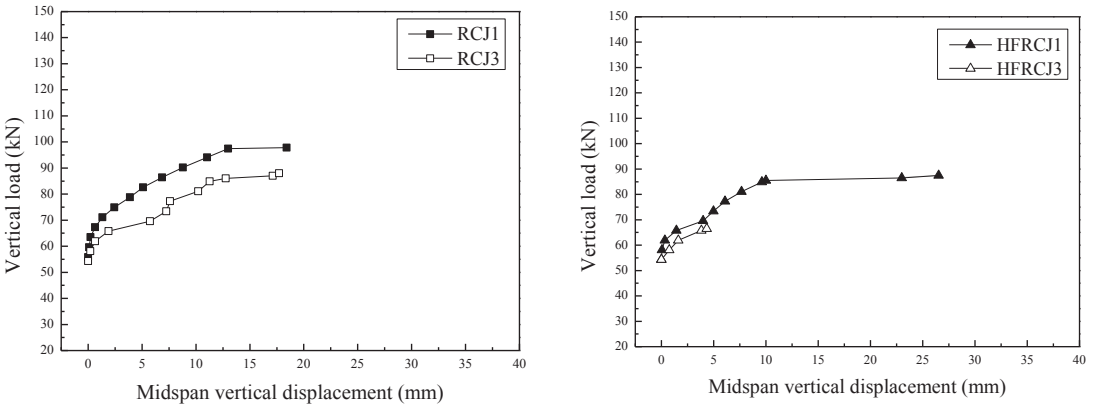

(a) Vertical load vs. vertical displacement

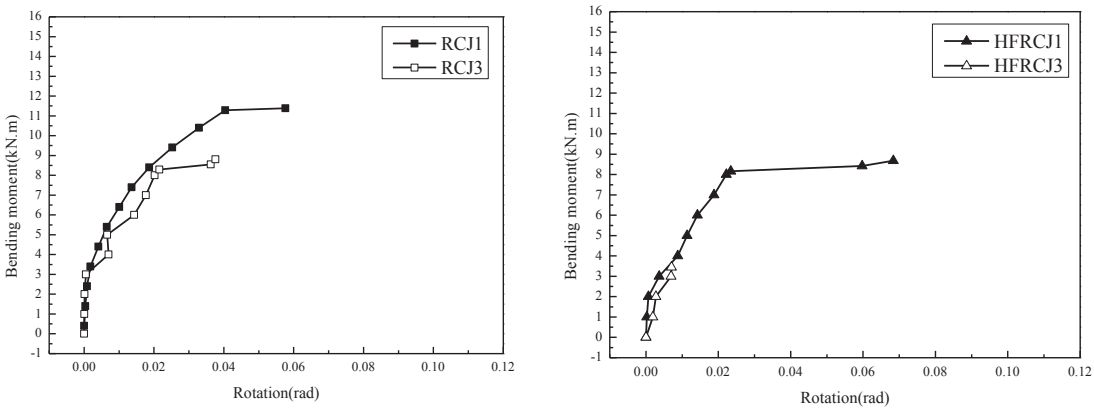

(b) Joint bending moment vs. rotation

Fig.14. Load vs. deformation curves for RCJ1 & RCJ3 and HFRCJ1 & HFRCJ3 (P_H=40 kN)

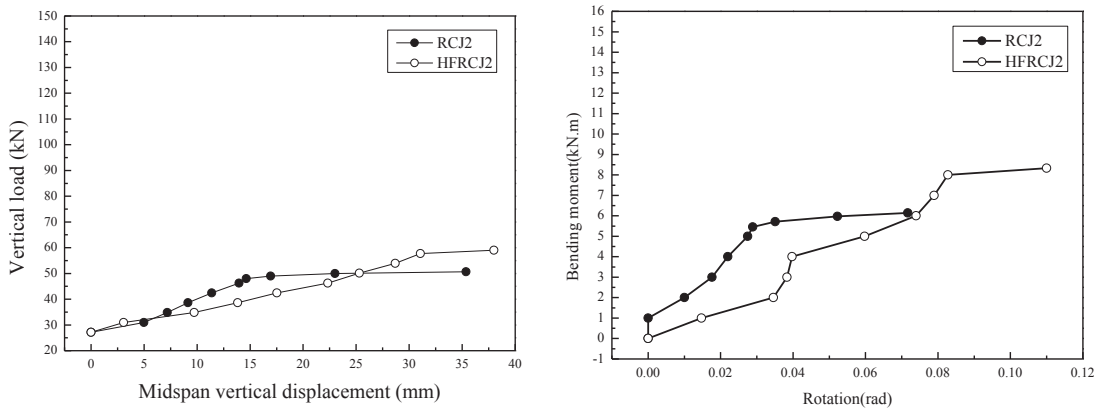

(a) RCJ2 & HFRCJ2, P_H=20 kN

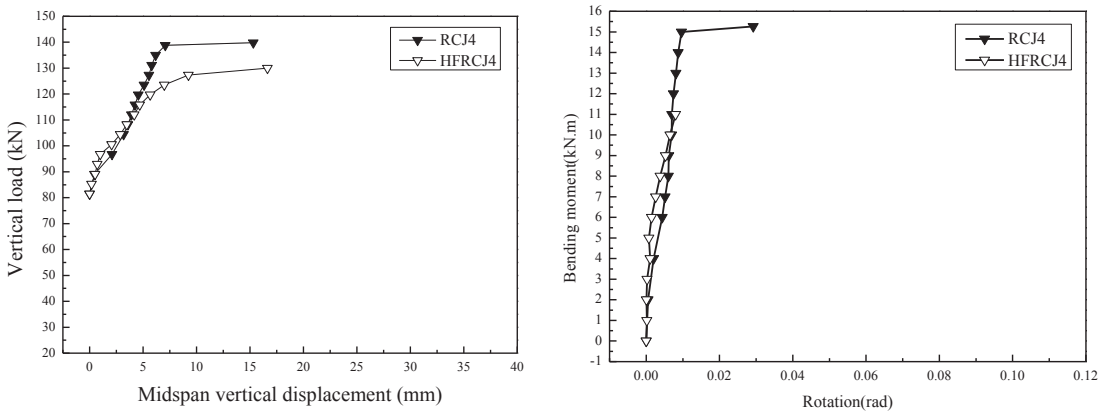

(b) RCJ4 & HFRCJ4, P_H=60 kN

Fig.15. Load vs. deformation curves for RCJ2 & HFRCJ2 and RCJ4 & HFRCJ4 (under-fire tests)

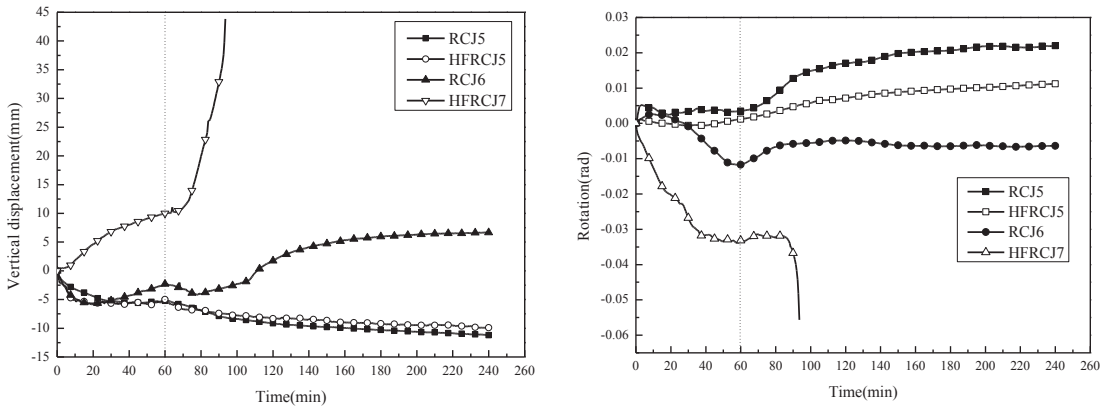

(a) Vertical deflection (b) Rotation

Fig.16. Deformation time histories during heating-cooling cycle for the post-fire cases

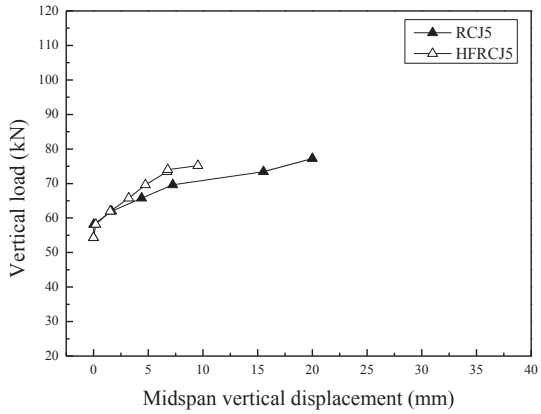

(a) Initial loading: M_c =2kNm P_H=40 kN

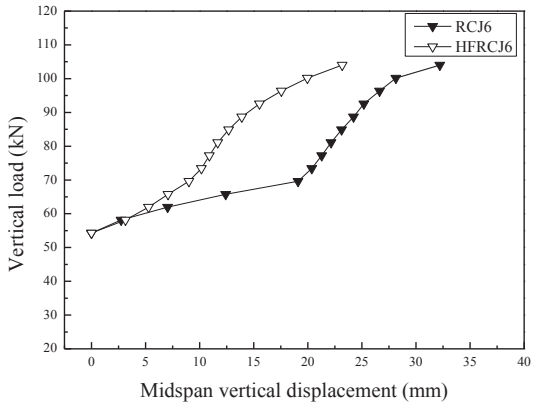

(b) Initial loading: M_c = -2kNm, P_H= 40 kN

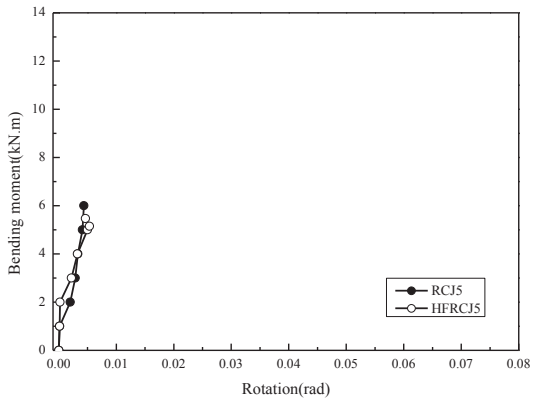

(c) Initial loading: M_c =2kNm P_H=40 kN

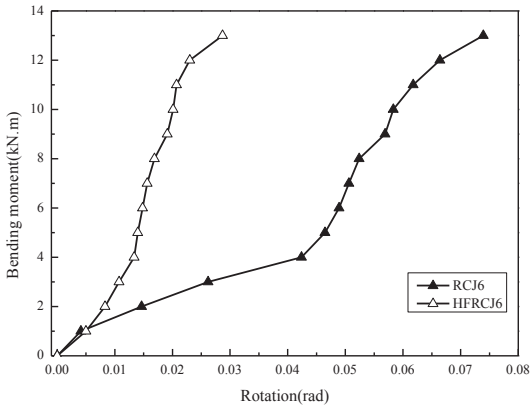

(d) Initial loading: M_c = -2kNm, P_H=40 kN

Fig.17. Load vs. deformation curves for the post-fire loading tests

(a) Joint concrete failure (RCJ5)

(b) Concrete fracture (HFRCJ5)

(c) Joint concrete failure (RCJ6)

(d) Concrete fracture (HFRCJ6)

Fig.18. Failure modes of specimens from post-fire loading tests

Table 1
Major tunnel fire accidents*

Year	Tunnel	Country	Fatalities and injured	Structure damage	Accident type
1968	Moorfleet	Germany	-	Serious damage on vault and side wall	Car accident
1994	Hugouenot	South Africa	59	Serious damage on tunnel lining	Bus accident
1994	Great Belt	Denmark	-	Widespread damage on tunnel region	Construction turnover
1996	Channel Tunnel	Britain-France	-	Widespread damage on tunnel region	Cargo fire
1999	Mont Blanc	France-Italy	38	Serious damage on tunnel lining	Cargo fire
1999	Tauren	Austria	12	Serious spalling on tunnel lining	Multi-car collision
2001	Gothard	Switzerland	21	Part of tunnel vault collapsed	Two trucks collision
2002	A86 Road Tunnel	France	-	Serious spalling on tunnel lining	Construction turnover
2004	Takayama	Japan	5	Surface concrete damage	Collision
2005	Fréjus	France-Italy	23	Serious damage on tunnel lining	Car accident
2011	Xinqingdaoliang	China	5	Widespread damage on tunnel region	Shunt
2014	Yanhou	China	31	Serious damage on tunnel lining	Collision

* This list is based on data from the following sources: Cafaro and Bertola (2010), Haack (2002), Haack (2004), ITA (2005), Khoury (2000); Kim et al. (2010), Leitner (2001), Park et al. (2006), Schrefler et al. (2002), Vianello et al. (2012)

Table 2
Concrete composition of the RC tunnel linings used in the tests

Item	kg/m^3
Portland cement	386
Aggregate	1143
Sand	640
Fly ash	74
Water	155
Admixture	5.5

Table 3
Properties of polypropylene fiber

Item	Value
Specific gravity	0.91
Length (mm)	12
Diameter (μm)	18
Tensile strength (MPa)	365
Elastic modulus (MPa)	3300
Melting point (˚C)	160
Ignition Point (˚C)	590
Alkali, acid and salt resistance	High

Table 4
Properties of steel fiber

Item	Value
Specific gravity	7.8
Length (mm)	50
Diameter (mm)	0.9
Tensile strength (MPa)	1000
Elastic modulus (MPa)	200000
Melting point (˚C)	1370

Table 5

Details of the test arrangement and key test results

No.	Age (day)	Initial boundary conditions	Designed loading case	Fire load	Failure mode	M_{max} (kNm)
RCJ1	321	M_c=0, P_H=40 kN	LC0	-	Joint bolts yielding	M_c=11.38
RCJ2	226	M_c =0, P_H=20 kN	LC1	HC	Joint bolts yielding	M_c=6.14
RCJ3	251	M_c =0, P_H=40 kN	LC1	HC	Joint bolts yielding	M_c=9.04
RCJ4	223	M_c =0, P_H=60 kN	LC1	HC	Joint concrete failure	M_c=15.26
RCJ5	540	M_c =2kN.m, P_H=40 kN	LC2	HC	Joint concrete failure	M_c=6
RCJ6	264	M_c =-2kN, P_H=40 kN	LC2	HC	Joint concrete failure	M_c=13
HFRCJ1	255	M_c =0, P_H=40 kN	LC0	-	Joint bolts yielding	M_c=8.68
HFRCJ2	312	M_c =0, P_H=20 kN	LC1	HC	Joint bolts yielding	M_c=8.33
HFRCJ3	176	M_c =0, P_H=40 kN	LC1	HC	Segment failure	M_c=3.45
HFRCJ4	278	M_c =0, P_H=60 kN	LC1	HC	Segment failure	M_c=12.7
HFRCJ5	282	M_c =2kN.m, P_H=40 kN	LC2	HC	Segment failure	M_c=5.4648
HFRCJ6	271	M_c =-2kN, P_H=40 kN	LC2	HC	Segment failure	M_c=13
HFRCJ7	269	M_c =-4kN, P_H=40 kN	LC2	HC	Segment failure	-

Note: M_c = bending moment at joint (centre of specimen)

Table 6

Summary of simple calculations for the yield / ultimate bending moments at ambient temperature

(a) Segmental joint (RC & HFRC)

Axial force	Failure mode	M_{max} (kNm)
P_H =20 kN	Joint bolts yielding	M_c=8.2
P_H =40 kN	Joint bolts yielding	M_c=10.4
P_H =60 kN	Joint bolts yielding	M_c=11.6
P_H =60 kN	Joint concrete crushing	M_c=9.0

(b) RC section

Axial force	Failure mode	M_{max} (kNm)
P_H =20 kN	Tensile reinforcement yielding	M_c=17.0
P_H =40 kN	Tensile reinforcement yielding	M_c=18.2
P_H =60 kN	Tensile reinforcement yielding	M_c=19.4

(c) HFRC section

Axial force	Failure mode	M_{max} (kNm)
P_H =20 kN	Tensile concrete cracking	M_c=8.0
P_H =40 kN	Tensile concrete cracking	M_c=8.4
P_H =60 kN	Tensile concrete cracking	M_c=8.8